SSRG International Journal of Mechanical Engineering
ISSN: 2348-8360/ https://doi.org/10.14445/23488360/IJME-V13I6P101

Volume 13 Issue 6, 1-18, June 2026


*Original Article*

# Variation Ride Comfort of a Converted Electric Vehicle Using 6 DOF Vehicle Vibration Model

Carlos Chunga Calcina[1], Christian Chunga Calcina[1], Yuri Silva Vidal[1], Juan Cutipa Luque[1], Waygand Beltran Quispe[1*], André Abelardo Tavares[2], Claudio Ponce Saldias[3], Christofer Diaz Arapa[1]

[1]*Universidad Nacional de San Agustín de Arequipa, Arequipa, Perú*
[2]*Centro Universitario SATC, Criciúma, Brazil.*
[3]*Universidade Federal de Santa Catarina: Florianópolis, Santa Catarina, Brazil.*

[1]*Corresponding Author : wbeltranq@unsa.edu.pe*

Received: 02 March 2026 Revised: 03 April 2026 Accepted: 05 May 2026 Published: 27 June 2026

***Abstract*** *- This study evaluates the changes in ride comfort in a Ford Ka after an electric vehicle conversion. The Ford Ka was selected because of its strong presence in the Brazilian market, making it a representative example for large-scale retrofit programs. Changing the combustion engine with an electric motor and battery pack changes the vehicle's mass distribution, modifying its vertical dynamic behavior and the vibration levels experienced by occupants. A six degree of freedom (6-DOF) half vehicle model was constructed in MATLAB/Simulink to simulate the vertical dynamics of the vehicle body, the front and rear unsprung masses and both seating points. Four road excitation cases were simulated: the positive and negative step inputs, a sinusoidal input, and a speed reducer input. Vertical acceleration data at each seat position were processed using the ISO 2631-1 Wk frequency weighting filter, and ride comfort was evaluated using the weighted Root Mean Square Acceleration (RMS) and the Vibration Dose Value (VDV). Both indicators increased after conversion across most scenarios, with the rear seat showing the most pronounced changes. VDV rose by up to 17.5% under sinusoidal excitation, while RMS increases of 15-25% were recorded depending on seating position and excitation type. These findings show that the stock suspension, calibrated for the original combustion-engine configuration, is no longer adequate after retrofitting and that suspension retuning should be treated as a required step in any serious electric conversion program.*

***Keywords*** *- Ride Comfort, ISO 2631-1, Half-Car Model, Vehicle electrification, Wk Weighting, RMS, VDV.*

## 1. Introduction

The transition to electric mobility is a complex and gradual process, requiring significant time, investment, and ongoing technological advancement. This progression varies across regions due to differences in economic, industrial, and infrastructural contexts. In this setting, the conversion of conventional vehicles to electric propulsion has emerged as a pragmatic approach, facilitating electrification without necessitating the complete replacement of the existing vehicle fleet. Currently, Hybrid Electric Vehicles (HEVs) and Battery Electric Vehicles (EVs) are widely regarded as key enablers of an eco-friendlier transportation system, as they reduce dependence on fossil fuels and mitigate harmful emissions [1]. However, the high acquisition cost of new electric vehicles remains a major barrier to their broad acceptance. Under these conditions, converting an Internal Combustion Engine (ICE) vehicle into an Electric Vehicle (EV) represents a technically viable and economically attractive alternative, primarily in regions where access to new electric platforms is limited [2]. For electrification strategies based on conversion to be relevant from an engineering perspective, the selected vehicle must be representative of the existing vehicle fleet. In this context, the Ford Ka has historically been one of the best-selling compact vehicles in Brazil, particularly during the second half of the 2010s.

Historical registration records from 2015 to 2020 confirm that the Ford Ka established itself as one of the best-selling models within the Brazilian hatchback segment, even during periods of economic instability [3-7]. As illustrated in Figure 1, this sustained market presence is further evidenced by its continued competitiveness in the used vehicle market through 2021, the year production ceased. Additionally, Table 1 presents the ranking of the top 10 used hatchback vehicles in Brazil, showing that the Ford Ka consistently maintained a competitive position over time. Taken together, these findings highlight the model's strong representativeness within the active compact vehicle fleet, supporting its selection as a suitable platform for electric conversion (retrofitting) studies. Consequently, the engineering results derived from its analysis are more likely to be applicable to large-scale retrofitting scenarios.

**Table 1. Top 10 classification of used hatchback vehicles (4–8 years old) in brazil**

| Position | 0 to 3 years | Score | 4 to 8 years | Score | 9 to 12 years | Score | 13 years or more | Score |
|---|---|---|---|---|---|---|---|---|
| 1 | Chevrolet Onix | 81 | Chevrolet Onix | 80.9 | Fiat Palio | 72.5 | Volkswagen Gol | 80.9 |
| 2 | Hyundai HB20 | 56.6 | Hyundai HB20 | 50.7 | Chevrolet Onix | 65.6 | Fiat Palio | 58.6 |
| 3 | Volkswagen Polo | 55.8 | Ford Ka | 50.1 | Hyundai HB20 | 61.2 | Chevrolet Corsa | 52.6 |
| 4 | Fiat Mobi | 52.8 | Volkswagen Gol | 47.8 | Volkswagen Gol | 60 | Fiat Uno | 51.4 |
| 5 | Fiat Argo | 51.8 | Fiat Argo | 47.5 | Fiat Uno | 53.5 | Chevrolet Celta | 50.3 |
| 6 | Renault Kwid | 48.1 | Volkswagen Polo | 46.5 | Ford Fiesta | 53.3 | Ford Fiesta | 45 |
| 7 | Volkswagen Gol | 44.3 | Renault Kwid | 46.4 | Renault Sandero | 51.2 | Volkswagen Fox | 43.3 |
| 8 | Peugeot 208 | 44.3 | Fiat Mobi | 44.3 | Volkswagen Fox | 50 | Ford Ka | 41.7 |
| 9 | Toyota Yaris | 41.3 | Renault Sandero | 42.9 | Ford Ka | 48.1 | Honda Fit | 40.2 |
| 10 | BYD Dolphin | 40.7 | Toyota Etios | 41.3 | Toyota Etios | 47.4 | Chevrolet Astra | 39.6 |

Note: Source: Used Vehicle Index (IVU), developed by Data OLX Autos in collaboration with FENAUTO (August 2025 Report). The data confirms the high demand and relevance of the Ford Ka (3rd place) in the secondary market, justifying its selection as a case study for the electrification process (retrofitting).

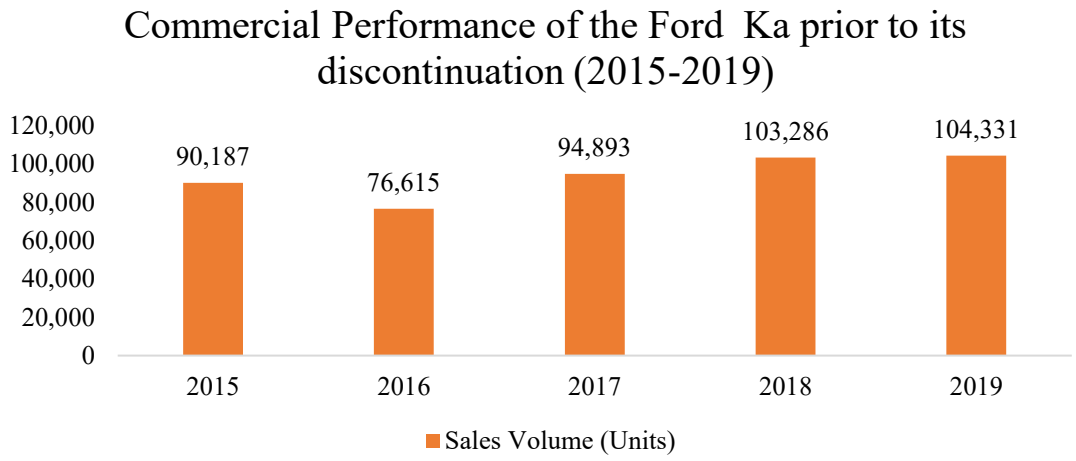


**Fig. 1 Annual sales volume and market ranking position of the Ford Ka in Brazil (2015–2019), based on national registration data [3-7]**

In the conversion process of a standard vehicle to electric propulsion, the total vehicle mass and how its mass is distributed are significantly altered. These changes cause mass variation effects that significantly impact the vertical dynamics of the vehicle and suspension performance [8]. Changes in mass distribution modify the system's natural frequencies, changing vibration transmission paths. Consequently, dynamic analysis is necessary in advance of the conversion process to avoid an unexpected reduction in performance [9]. In addition, the conversion process has a direct effect on ride comfort, which is characterized by the human psycho physiological response to full-body vibration [10, 11]. These vibrations result from various sources, including road surface irregularities, aerodynamic effects, imbalance in the wheel and mechanical components, with road-induced vibrations being the main contribution [11]. The literature presents various modeling strategies for the ride comfort analysis in vehicles. Among these, the quarter vehicle model with two degrees of freedom corresponds to the most basic model, representing the main vertical dynamics of the

sprung and unsprung components [12, 13]. This model has been extensively applied to study the effect of suspension parameters on comfort during ride and road holding performance [13, 14].

However, the quarter car model does not consider multi-directional dynamics, such as the pitching and rolling, and ignores complex components like control arms or wheel rotation [12, 15]. In addition, this model typically assumes idealized paths on level surfaces with zero steering angles [16]. Due to these limitations, a move toward more advanced formulations is essential to account for the coupled rotational vibrations that impact passenger comfort in vehicles [15].

The half-car model addresses many of these limitations by including pitch dynamics in addition to the vertical dynamic responses of both axles [15, 17]. It has been widely applied in this study how suspension configuration impacts load distribution transfer, ride comfort, and vehicle stability [15], and it generally performs better than the quarter car model in the calculation of RMS acceleration, the principal parameter in ride comfort standards [18].

Still, this formulation is restricted to longitudinal and vertical directions [15]. It does not capture lateral rolling motion [15]. While it can also present reduced precision than that of the quarter car model during isolated obstacles, such as individual road bumps. [15, 17].

The complete vehicle model corresponds to the most complete lumped approach capable of representing complex dynamic responses in multiple directions, including combined pitch and roll motions [15]. By giving a realistic characterization of vibration propagation mechanism, this model obtains strong experimental reliability with errors in vertical aceleration commonly below 10%, reducing the typical overestimation in the basic formulation [18]. The main disadvantage is the excessive complexity of the model and the challenge of identifying the large number of required physical parameters, which increases computational demand.

In addition, during discrete excitations like single potholes, the accuracy is reduced because simpler 2 DOF models are able to obtain similar accuracy when predicting maximum passenger accelerations [15, 17]. As a result of investigations focused on vertical vibrations in vehicle retrofit applications, the half vehicle configuration presents the best balance between modeling precision and practical parameterization [15, 17].

The evolution of vehicle dynamic studies has moved from passive dynamic modeling to intelligent optimization methods and adaptive control [19-21]. Later research extended conventional frameworks by applying multi-objective techniques designed to balance passenger comfort together with handling in different excitation scenarios [20, 22]. In this context, computational methods including Genetic Algorithms (GA) and Particle Swarm Optimization (PSO) have been extensively employed to improve suspension settings, consolidating the importance of simplified models as standard baselines for robust system design. [17, 20, 21].

Recent advances have presented active and semi-active suspension systems providing simultaneous benefits in passenger comfort by dynamically controlling pitching and bouncing motions. These systems include sensors and actuators to control damping and stiffness properties during operation [13].

To deal with the intrinsic nonlinearities of these suspension systems, researchers are progressively applying Artificial Intelligence (Al) such as Neural Networks and Reinforcement Learning, allowing suspension systems to autonomously recognize road irregularities and avoid the need for extensive mathematical formulations of difficult road conditions [20].

Additionally, because the simultaneous optimization of mounting locations, kinematics restrictions, and geometric parameters (camber, caster, toe) is categorized as an NP hard problem, traditional computing methods frequently present excessive computational demand. [19, 20]. As a result, current investigations explore Quantum Computing to solve this limitation using parallel qubit processing [19].

Even with these developments, both Al and quantum-based optimization are only effective as the physical model supporting them [19]. In this case of ICE to EV conversion, precisely determining the new inertia and mass distribution is a necessary requirement before applying advanced control methods can be effectively applied.

In this context, this research presents a new methodology to analyze passenger comfort of a Ford Ka subjected to electric propulsion. By using a Six Degree of Freedom (6-DOF) half vehicle model, this research obtains an efficient balance between computational cost and modeling accuracy, making possible a dependable estimation of vertical dynamic acceleration responses at occupant contact locations based on ISO 2631 criteria [11, 23].

Additionally, this research indicates, as a first approach with a half vehicle formulation for the Ford Ka platform in particular, that the conversion from ICE to EV significantly modifies important physical properties, including distribution of mass and the vehicle's longitudinal inertia characteristics. By evaluating these variations under linear driving conditions, this research presents the necessary empirical basics to implement modern suspension technologies to the specific requirements of the EV retrofitting sector [24].

## 2. Electric Conversion of the Ford Ka (Innowattis Project)

The Innowattis Project is based on the conversion of a Ford Ka model 2009 originally using an internal combustion powertrain into an electric vehicle. The project was carried out at the Electric Mobility Center (NME) of the UNISATC University Center, located in Criciúma, SC, Brazil.

During the electrification process, the original combustion engine, gasoline, together with the transmission, were exchanged for a 16 CV (12 kW) electric motor, the power inverter system, along with a battery pack. Because of this, the retrofitted vehicle presents a mean power consumption of 0.21 kWh per kilometer. The electrical efficiency obtained achieves approximately 86% during city driving, with values up to 88.9% in highway driving.

The redistribution of vehicle mass caused by the electric motor and battery system changes the vehicle dynamic response suspension properties, together with natural frequencies, strongly modifying ride comfort and vertical response. As a result, evaluating the way changes in mass distribution and inertia influence how vibrations are transmitted from road disturbances into the passenger cabin is fundamental [25].

Consequently, the next sections analyze the passenger comfort of the retrofitted vehicle according to the standards of ISO 2631-1 [11, 27]. This regulation provides the principal international guideline by establishing standardized evaluation methods for evaluating full-body human exposure to mechanical vibrations, applying weighted vertical acceleration metrics, including Root Mean Square (RMS) acceleration, together with Vibration Dose Value (VDV) [23, 26].

The comfort levels described in ISO 2631-1 offer a standard reference that connects quantitative vibration measures with human subjective response using semantic discomfort scales [26, 27]. By applying these ISO 2631-1 standards ranges as the baseline reference, this study makes sure that the simulation outputs produced by the 6 DOF formulation can be contrasted with commonly accepted subjective comfort criteria, consequently, a generally accepted assessment of passenger comfort for the retrofitted vehicle [23, 26].

A comparison of the inertia properties of the conventional vehicle and the retrofitted electric vehicle is presented in the following section, illustrating the physical changes that explain the dynamic study conducted in this research. Table 2 shows the position of the center of gravity and the Inertia tensor properties of the Conventional Combustion (ICE) vehicle. In contrast, Table 3 shows the equivalent properties for the Electric Vehicle (EV) conversion.

**Table 2. Center of gravity location and inertia tensor properties of the conventional combustion (ICE) vehicle**

| **Total Weight** | | 1265 |
|---|---|---|
| **Center of Gravity (m)** | | |
| Xg | Yg | Zg |
| 1.425 | -0.03 | 0.526 |
| **INERTIA TENSOR MATRIX** | | |
| | X | Y |
| X | 62 | 65 |
| Y | 65 | 1000 |
| Z | 4 | 2 |

**Table 3. Center of gravity position and inertia tensor properties of the converted Electric Vehicle (EV)**

| **Total Weight** | | 1274.5 |
|---|---|---|
| **Center of Gravity (m)** | | |
| Xg | Yg | Zg |
| 1.417 | -0.001 | 0.503 |
| **INERTIA TENSOR MATRIX** | | |
| | X | Y |
| X | 81 | 2 |
| Y | 2 | 812 |
| Z | 39 | 1 |

Figure 2 presents an isometric profile representation of the converted Ford Ka vehicle, showing the hood open, illustrating the component distribution of the principal components after the conversion process.

Figure 3 presents in detail the electric drivetrain arrangement in the motor compartment, showing the integration of the electric motor. These structural modifications, documented during the conversion process, are directly responsible for the observed changes in mass distribution and the subsequent shift in the vehicle's center of gravity.

**Fig. 2 Converted Ford Ka (Innowattis project) developed at SATC**

**Fig. 3 Electric motor and powertrain components of the Innowattis project**

## 3. Six-Degree-of-Freedom Vehicle Vibration Model

The vibration model proposed in this study consists of a sprung mass, corresponding to the vehicle body. $m_c$, coupled with two unsprung masses representing the front and rear wheels, denoted as $m_{uf}$ and $m_{ur}$, respectively. In addition, two secondary masses associated with the front and rear seats, denoted as $m_{sf}$ and $m_{sr}$ , are included to account for the dynamic interaction between the occupants and the vehicle structure.

Figure 4 illustrates the Free-Body Diagram (FBD), showing the interactions between the sprung masses, unsprung masses, seat masses, and the suspension stiffness and damping elements. This half-car configuration, including the seat dynamics, follows the established standards used in previous vibration studies [18, 28].

The system shows six degrees of freedom. Two degrees of freedom are associated with the vertical displacements of the front and rear wheels [29]. Two additional degrees of freedom correspond to the vertical displacements of the front and rear seats. One degree of freedom describes the vertical motion of the vehicle's center of gravity, and the remaining degree of freedom represents the pitch motion of the vehicle body about the lateral axis [30].

The road irregularities that excite the system are applied at the front and rear wheels and are represented by the input profiles. $X_f(t)$ and $X_r(t)$. It is important to note that the stiffness and damping coefficients associated with the seat systems ($k_f, k_r, c_f$ and $c_r$) were adopted from reference [31], while all remaining parameters were measured directly on the vehicle. The definitions and numerical values of the fixed parameters used in the model are presented in Table 4, whereas the variable parameters are detailed in Table 5.

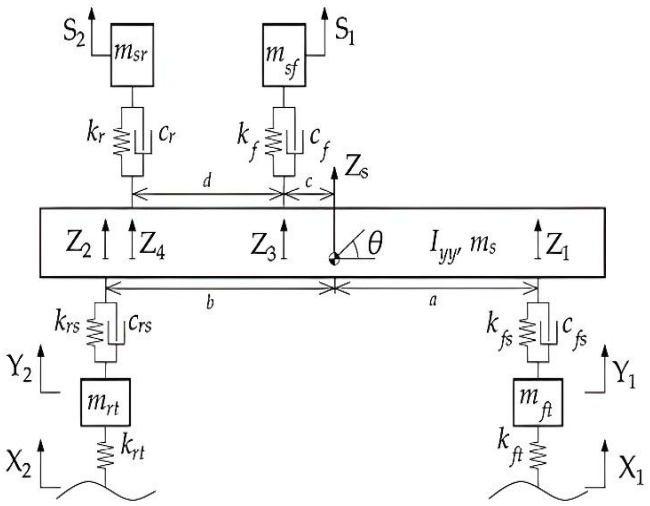


**Fig. 4 Free-body diagram of the 6-DOF vehicle vibration model**

The displacement vector is defined as follows:

$$q(t) = \begin{bmatrix} Z_s(t) \\ \theta(t) \\ Z_{uf}(t) \\ Z_{ur}(t) \\ S_1(t) \\ S_2(t) \end{bmatrix} = \begin{bmatrix} Sprung\ mass\ C.G.\ (m) \\ Pitch\ angle\ (rad) \\ Front\ unsprung\ mass(m) \\ Rear\ unsprung\ mass\ (m) \\ Front\ seat\ displacement\ (m) \\ Rear\ seat\ displacement\ (m) \end{bmatrix} \quad (1)$$

Geometric parameters and relationships used in the model are defined as follows:

- $Z_1 = Z_s + a\theta$ (front chassis point)
- $Z_2 = Z_s - b\theta$ (rear chassis point)
- $Z_3 = Z_s - c\theta$ (front seat body connection)
- $Z_4 = Z_s - d\theta$ (rear seat body connection)

The linearized dynamic equation is expressed in matrix form as follows:

$$M\ddot{q}(t) + C\dot{q}(t) + Kq(t) = G(t) \quad (2)$$

### *3.1. Definition of Matrices and Excitation Vector*

The general linearized equation of motion of the vehicle (2) is developed through the definition of the matrices that represent the physical properties of the system.

#### *3.1.1. Mass matrix M*

The mass matrix M is a fundamental component of the system's governing equations of motion, as it characterizes the vehicle's inertial properties. This matrix contains the terms associated with the lumped masses of the system, representing the main body, the occupants, and the unsprung masses, along with their respective moments of inertia with respect to the transverse axis (pitch).

In the Six-Degree-of-Freedom (6-DOF) model, matrix M is defined as a diagonal matrix, assuming that the coordinate system is aligned with the principal axes of inertia, which simplifies the decoupling of the equations. Its general form, which accounts for the redistribution of mass following the electric conversion, is expressed as follows:

$$M = \begin{bmatrix} m_c & 0 & 0 & 0 & 0 & 0 \\ 0 & I_{yy} & 0 & 0 & 0 & 0 \\ 0 & 0 & m_{uf} & 0 & 0 & 0 \\ 0 & 0 & 0 & m_{ur} & 0 & 0 \\ 0 & 0 & 0 & 0 & m_{sf} & 0 \\ 0 & 0 & 0 & 0 & 0 & m_{sr} \end{bmatrix} \quad (3)$$

*3.1.2. Stiffness Matrix K*

The stiffness matrix K relates the displacements of each degree of freedom to the elastic forces generated in the suspension and seat springs. Its general formulation is expressed as:

$$K = \begin{bmatrix} K_{11} & K_{12} & K_{13} & K_{14} & K_{15} & K_{16} \\ K_{12} & K_{22} & K_{23} & K_{24} & K_{25} & K_{26} \\ K_{13} & K_{23} & K_{33} & 0 & 0 & 0 \\ K_{14} & K_{24} & 0 & K_{44} & 0 & 0 \\ K_{15} & K_{25} & 0 & 0 & K_{55} & 0 \\ K_{16} & K_{26} & 0 & 0 & 0 & K_{66} \end{bmatrix} \quad (4)$$

$$K_{11} = k_{fs} + k_{rs} + k_f + k_r$$
$$K_{12} = -k_f c - k_r d + k_{fs} a - k_{rs} b$$
$$K_{13} = -k_{fs} \;\; ; \;\; K_{14} = -k_{rs}$$
$$K_{15} = -k_f \;\; ; \;\; K_{16} = -k_r$$
$$K_{22} = k_{fs} a^2 + k_{rs} b^2 + k_f c^2 + k_r d^2$$
$$K_{23} = -k_{fs} a \;\; ; \;\; K_{24} = +k_{rs} b$$
$$K_{25} = +k_f c \;\; ; \;\; K_{26} = +k_r d$$
$$K_{33} = k_{fs} + k_{tf} \;\; ; \;\; K_{44} = k_{rs} + k_{tr}$$
$$K_{55} = k_f \;\; ; \;\; K_{66} = k_r$$

**Note:** The matrix is symmetric; the zeros indicate that there are no direct couplings between the wheel and seat degrees of freedom.

*3.1.3. Damping Matrix C*

The damping matrix **C** includes the viscous coefficients of the suspension and seat dampers and represents the energy dissipation within the system. Its general form is analogous to that of the stiffness matrix:

$$C = \begin{bmatrix} C_{11} & C_{12} & C_{13} & C_{14} & C_{15} & C_{16} \\ C_{12} & C_{22} & C_{23} & C_{24} & C_{25} & C_{26} \\ C_{13} & C_{23} & C_{33} & 0 & 0 & 0 \\ C_{14} & C_{24} & 0 & C_{44} & 0 & 0 \\ C_{15} & C_{25} & 0 & 0 & C_{55} & 0 \\ C_{16} & C_{26} & 0 & 0 & 0 & C_{66} \end{bmatrix} \quad (5)$$

$$C_{11} = c_{fs} + c_{rs} + c_f + c_r$$
$$C_{12} = -c_f c - c_r d + c_{fs} a - c_{rs} b$$
$$C_{13} = -c_{fs} \;\; ; \;\; C_{14} = -c_{rs}$$
$$C_{15} = -c_f \;\; ; \;\; C_{16} = -c_r$$
$$C_{22} = c_{fs} a^2 + c_{rs} b^2 + c_f c^2 + c_r d^2$$
$$C_{23} = -c_{fs} a \;\; ; \;\; C_{24} = +c_{rs} b$$
$$C_{25} = +c_f c \;\; ; \;\; C_{26} = +c_r d$$
$$C_{33} = c_{fs} + c_{tf} \;\; ; \;\; C_{44} = c_{rs} + c_{tr}$$
$$C_{55} = c_f \;\; ; \;\; C_{66} = c_r$$

*3.1.4. Excitation vector G*

The road profiles $X_1(t)$ and $X_2(t)$ generate dynamic forces that are transmitted through the tire–suspension system to the vehicle structure. This formulation represents an equivalent force-based input, commonly adopted in linearized vehicle vibration models.

By grouping the stiffness and damping terms associated with these interactions, the excitation vector is expressed as:

$$G(t) = \begin{bmatrix} k_{tf} X_1(t) + k_{tr} X_2(t) \\ a k_{tf} X_1(t) - b k_{tr} X_2(t) \\ k_{tf} X_1(t) \\ k_{tr} X_2(t) \\ 0 \\ 0 \end{bmatrix} + \begin{bmatrix} c_{tf} \dot{X}_1(t) + c_{tr} \dot{X}_2(t) \\ a c_{tf} \dot{X}_1(t) - b c_{tr} \dot{X}_2(t) \\ c_{tf} \dot{X}_1(t) \\ c_{tr} \dot{X}_2(t) \\ 0 \\ 0 \end{bmatrix} \quad (6)$$

$X_1(t)$ and $X_2(t)$ are the vertical displacement inputs of the road profile applied at the front and rear wheel positions, respectively.

**Table 4. Fixed parameters of the 6-DOF vehicle vibration model**

| Parameters | Definitions | Values |
|---|---|---|
| $m_{sf}$ | mass of 1 person and a front seat | 85 kg |
| $m_{sr}$ | mass of 1 person and a rear seat | 84 kg |
| $m_{uf}$ | mass of 1 front wheel | 11 kg |
| $m_{ur}$ | mass of 1 rear wheel | 11 kg |
| $k_f$ | front seat spring stiffness coefficient | 15,000 N/m |
| $k_r$ | rear seat spring stiffness coefficient | 15,000 N/m |
| $k_{fs}$ | front suspension stiffness coefficient | 15,800 N/m |
| $k_{rs}$ | rear suspension stiffness coefficient | 15,800 N/m |
| $k_{tf}$ | front tire spring stiffness coefficient | 180,000 N/m |
| $k_{tr}$ | rear tire spring stiffness coefficient | 180,000 N/m |
| $c_f$ | front seat damping coefficient | 500 N-s/m |
| $c_r$ | rear seat damping coefficient | 500 N-s/m |
| $c_{fs}$ | front suspension damping coefficient (tension - compression) | 2200 - 650 N-s/m |
| $c_{rs}$ | rear suspension damping coefficient (tension - compression) | 2200 - 650 N-s/m |

Note: The seat masses include a representative occupant mass, assumed constants for all simulations. This assumption corresponds to standard practices widely adopted in vehicle vibration and ride comfort studies [26, 28].

**Table 5. Variable parameters of the 6-DOF vehicle vibration model**

| Parameters | Definitions | Unmodified vehicle | Modified vehicle |
|---|---|---|---|
| $m_c$ | half car body mass | 441.50 kg | 446.25 kg |
| $I_{yy}$ | Half-car moment of inertia | 423.45 kg-m2 | 328.29 kg-m2 |
| $a$ | distance from the front tire to the body center of gravity | 1.2550 m | 1.2466 m |
| $b$ | distance from rear tire to body center of gravity | 1.1650 m | 1.1734 m |
| $c$ | distance from the front seat to the body center of gravity | 0.2568 m | 0.2651 m |
| $d$ | distance from the rear seat to the body center of gravity | 1.0289 m | 1.0373 m |

Note: An equivalent damping value was adopted for simulations based on Table 4.

The mathematical representation of the 6-DOF vibration model requires the definition of both invariant structural properties and those subject to change due to the electrification process. Table 4 summarizes the fixed parameters, including stiffness and damping coefficients for the seats, tires, and suspension systems, which are assumed to remain constant for both vehicle configurations. In contrast, mass redistribution and the relocation of the Center of Gravity (CG) require adjustments of specific inertial and geometric variables. These modifications, comparing the unmodified Internal Combustion Engine Vehicle (ICEV) with the converted Electric Vehicle (EV), are detailed in Table 5. These values serve as the primary input for the numerical simulations to determine the vertical dynamic response of the system.

### *3.2. Equations of Motion*

Starting from the general matrix formulation presented in Equation (2), the scalar expressions corresponding to each degree of freedom of the Half-Car model are developed below. These equations describe the dynamic equilibrium of the sprung mass, the pitch moment, and the vertical displacements of the unsprung masses and seats [32]. The derivations are obtained by applying Newton's second law together with the geometric linearization for small rotations. In the matrix formulation, the coordinates of the unsprung masses are denoted as $Z_{uf}$ and $Z_{uf}$ to maintain uniformity within the state vector, being equivalent to $Y_1$ and $Y_2$ as represented in Figure 4.

Vertical motion of the vehicle CG is formulated as follows:

$$\begin{aligned} m_s\ddot{Z}_s = {} & k_f(S_1 - Z_3) + c_f\left(\dot{S} - \dot{Z}_3\right) + k_r(S_2 - Z_4) \\ & + c_r\left(\dot{S}_2 - \dot{Z}_4\right) - k_{fs}(Z_1 - Y_1) \\ & - c_{fs}\left(\dot{Z}_1 - \dot{Y}_1\right) - k_{rs}(Z_2 - Y_2) \\ & - c_{rs}(\dot{Z}_2 - \dot{Y}_2) \end{aligned} \tag{7}$$

The pitch motion of the sprung mass, centered at the vehicle's CG, is described by the following differential equation:

$$\begin{aligned} I_{yy}\ddot{\theta} = {} & \left[k_{rs}(Z_2 - Y_2) + c_{rs}\left(\dot{Z}_2 - \dot{Y}_2\right)\right]b \\ & - \left[k_{fs}(Z_1 - Y_1) + c_{fs}\left(\dot{Z}_1 - \dot{Y}_1\right)\right]a \\ & - \left[k_f(S_1 - Z_3) + c_f\left(\dot{S}_1 - \dot{Z}_3\right)\right]c \\ & - [k_r(S_2 - Z_4) - c_r(\dot{S}_2 - \dot{Z}_4) \end{aligned} \tag{8}$$

The differential equation for vertical motion of the front wheel is :

$$\begin{aligned} m_{ft}\ddot{Y}_1 = {} & k_{ft}(X_1 - Y_1) + k_{fs}(Z_1 - Y_1) \\ & + c_{fs}\left(\dot{Z}_1 - \dot{Y}_1\right) \end{aligned} \tag{9}$$

Vertical motion of the rear wheel is governed by:

$$\begin{aligned} m_{rt}\ddot{Y}_2 = {} & k_{rt}(X_2 - Y_2) + k_{rs}(Z_2 - Y_2) \\ & + c_{rs}\left(\dot{Z}_2 - \dot{Y}_2\right) \end{aligned} \tag{10}$$

Vertical motion of the front seat is described as:

$$m_{fs}\ddot{S}_1 = k_f(Z_3 - S_1) + c_f\left(\dot{Z}_3 - \dot{S}_1\right) \tag{11}$$

Vertical motion of the rear seat is formulated as follows:

$$m_{rs}\ddot{S}_2 = k_r(Z_4 - S_2) + c_r\left(\dot{Z}_4 - \dot{S}_2\right) \tag{12}$$

where $Y_i$ , $Z_s$ , $Z_i$ , $S_i$ , and $\theta$ are the vertical displacements of the tires, the sprung-mass center of gravity, the sprung mass at points $i$, the seats, and the pitch motion, respectively. Moreover, $\dot{Y}_i$ , $\dot{Z}_s$ , $\dot{S}_i$ and $\dot{\theta}$ represent the corresponding vertical velocities and pitch velocity. Likewise, $\ddot{Y}_i$ , $\ddot{Z}_s$ , $\ddot{S}_i$ and $\ddot{\theta}$ denote the vertical and pitch accelerations, respectively. Finally, $X_1$ and $X_2$ represent the road-induced excitation inputs.

#### *3.2.1. Road Profiles for Testing*

To evaluate the ride comfort of the Ford Ka, four simulation cases are considered using different road excitation profiles. In the first and second cases, the road input is defined as a positive elevation of 0.075 m (Figure 5) and a negative elevation of −0.075 m (Figure 6), respectively.

In the third case, the road profile consists of a sinusoidal excitation composed of two consecutive depressions with depth $h = 0.075\ m$ and wavelength $\lambda = 3\ m$ as illustrated in Figure 7.

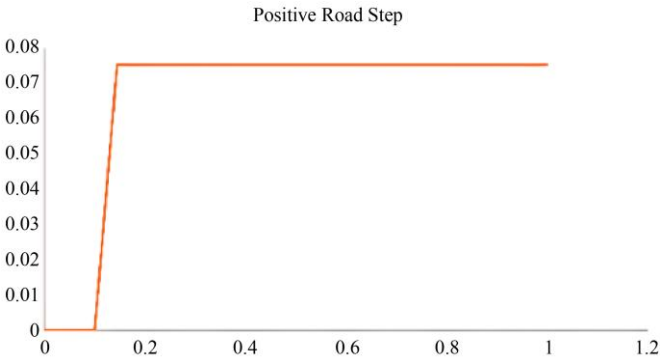


**Fig. 5 Road profile for the first test (positive elevation of 0.075 m)**

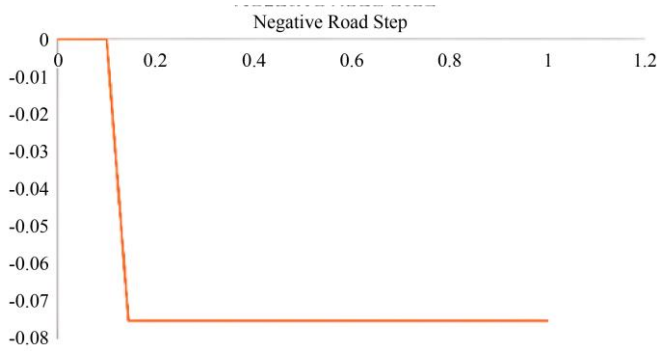


**Fig. 6 Road profile for the second test (negative elevation of −0.075 m)**

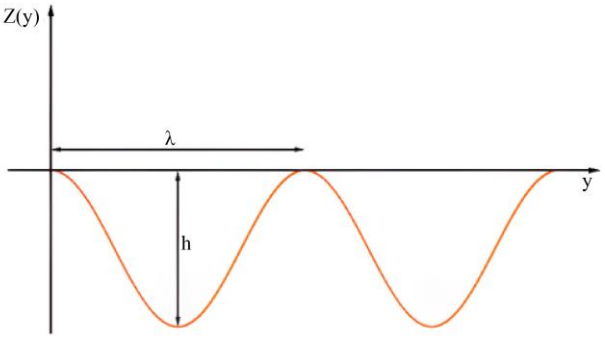


**Fig. 7 Road profile for the third test (sinusoidal road profile)**

Furthermore, for the tests, a vehicle speed of V=60km/h is assumed, and the rear tire is considered to follow the same trajectory as the front tire with a time delay $\tau = \frac{a+b}{V}$.

The road profile for the third test is expressed as a function of time by the following equations:

$$X_1 = \begin{cases} \frac{h}{2}\left(\cos\left(\omega(t-\tau)\right)-1\right), & if \quad 0 \le t \le \frac{2\lambda}{V} \\ 0 \quad , & otherwise \end{cases} \quad (13)$$

$$X_2 = \begin{cases} \frac{h}{2}\left(\cos\left(\omega(t-\tau)\right)-1\right), if\ 0 \le t \le \frac{2\lambda}{V}+\tau \\ 0 \quad , \quad otherwise \end{cases} \quad (14)$$

where the frequency is given by:

$$\omega = \frac{2\pi V}{\lambda} \quad (15)$$

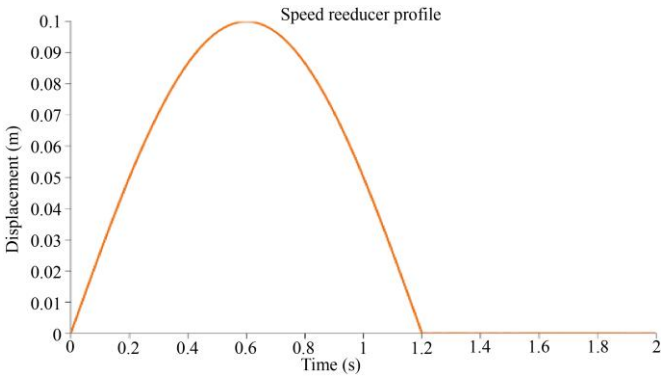


**Fig. 8 Road profile for the fourth test (speed reducer profile)**

Additionally, a fourth simulation scenario incorporates a speed bump profile based on the geometric standards and technical criteria established by the Ministry of Transport and Communications (MTC) of Peru [33]. These standards define critical parameters, such as height, length, and slope, according to the design speed of the road. The vertical road displacement for this specific case is defined by the following half-sine wave expression:

$$z_r(t) = \begin{cases} h \cdot \sin\left(\frac{\pi v}{L}\left(t-\frac{d}{v}\right)\right), if\ \frac{d}{v} \le t \le \frac{d+L}{v} \\ 0 \quad , \quad otherwise \end{cases} \quad (15)$$

Where $h = 0.1m$ and $L = 5\ m$ represent the height and length of the speed bump, respectively, $v$ is the constant vehicle speed 60 km/h, and $d = 0\ m$ is the distance from the start of the simulation to the beginning of the bump. These values were selected in accordance with the technical criteria for speed reducers [33].

*3.2.2. MATLAB/Simulink Model*

The mathematical model was implemented in MATLAB/Simulink to compare ride comfort before and after the vehicle conversion. The implementation of this simulation environment is validated by recent studies as a solid reference for vehicle vibration analysis. Based on the work of Alqam and Mnif, MATLAB/Simulink makes it possible to transform complicated differential equations into block-based modular diagrams, simplifying the investigation of vertical dynamic responses in various road scenarios with strong numerical reliability. This software platform is especially effective for studying how modifications in vehicle mass related to electric vehicle retrofits impact the transmissibility of the vehicle vibrations.

Additionally, studies by Nguyen et al. [35] and Srinivasan [36] confirm that multi-DOF models implemented using Simulink are fundamental for obtaining the required international accuracy criteria. These computational frameworks make possible the evaluation of comfort-related metrics, making sure that the vehicle dynamic response stays within permissible ranges after structural changes, including the addition of battery systems.

Figure 9 shows the simulation block diagram of the computational setup showing the propagation of signal from applied excitations inputs modeled as road surface irregularities to the system's outputs, including seat vertical acceleration responses and displacement of the center of gravity.

The excitation inputs correspond to profiles previously mentioned applied at the front and rear wheels, denoted as $X_1$ and $X_2$, respectively. A time delay between these inputs was introduced as a function of vehicle speed and wheelbase. For the simulations, a constant vehicle speed of 60 km/h was considered.

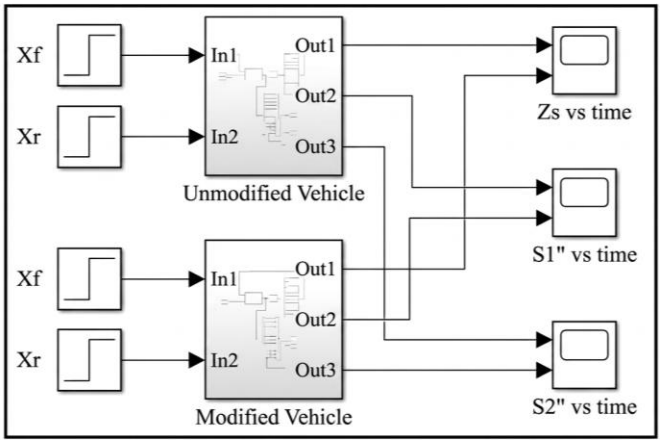


**Fig. 9 Flow chart of the vehicle vibration model**

## 4. Results Analysis

In the first test case, the vertical dynamic response of the vehicle to a positive road bump of +0.075 m was evaluated using a step-type input function in Simulink.

Figures 10 and 11 display the vertical dynamic responses at both front and rear seats in that order for the original configuration, together with the original vehicle and the converted EV.

In the two scenarios, a rapid acceleration rise can be observed right after the excitation and then followed by a vibration-damping process that slowly attenuates the vibration response. Comparing the configurations makes it possible to perform a direct analysis of the impact of the electric retrofit on the transmission of vibrations to the vehicle occupants.

As the acceleration responses of both configurations are close in amplitude and intersect in some regions, a difference signal (After − Before) was incorporated into every figure to simplify interpretation.

This extra signal makes it possible to better identify small changes in vibration intensity produced by changes in mass distribution without affecting the visualization of the original temporal responses.

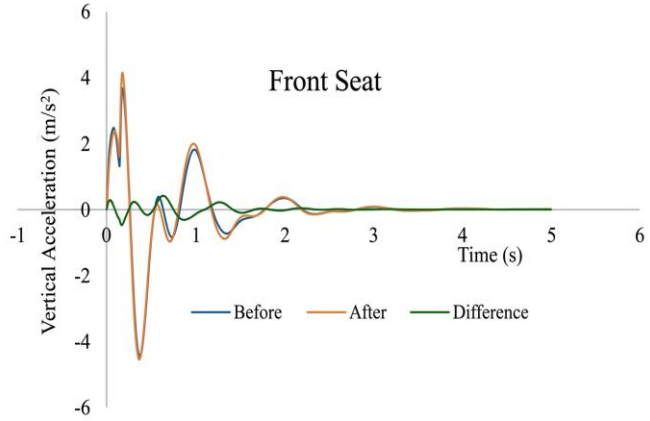


**Fig. 10 Vertical acceleration response at the front seating area due to a positive bump (before, after, and difference)**

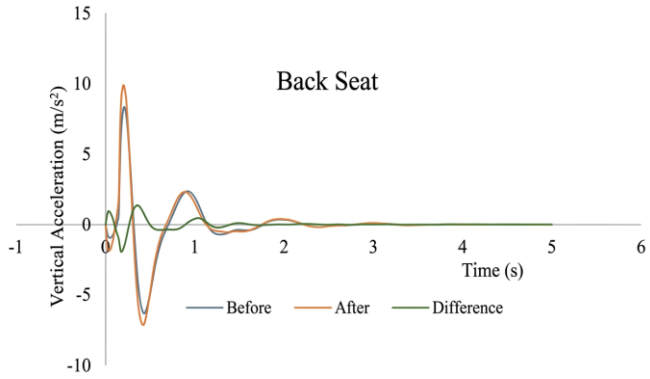


**Fig. 11 Vertical acceleration response at the rear seating area due to a positive bump (before, after, and difference)**

The second case applied a negative vertical road input of 0.075 m, simulating an abrupt depression in the road surface. Figures 12 and 13 present a comparison of the obtained vertical accelerations in the front and rear seating areas for both the conventional and converted vehicles.

The negative road input causes peak accelerations that are different in magnitude and occurrence time when compared with the positive excitation case. This analysis helps assess the suspension performance to reduce vibrations produced by holes and depressions in the road surface.

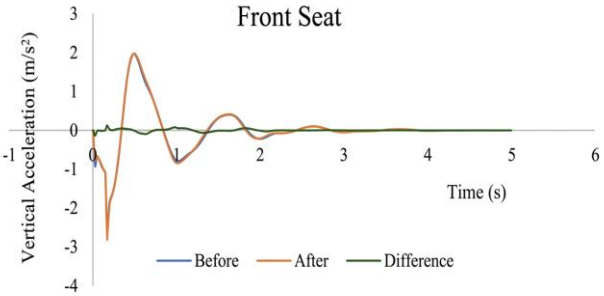


**Fig. 12 Vertical acceleration response at the front seating area due to a negative bump (before, after, and difference)**

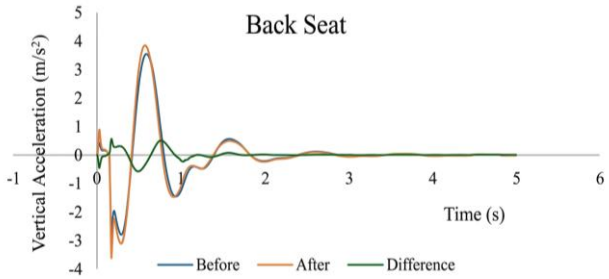


**Fig. 13 Vertical acceleration response at the rear seat due to a negative bump (before, after, and difference)**

During the third evaluation, a sinusoidal road profile was considered characteristic of a road with periodic irregularities or repetitive surface disturbance. This road input enables analysis of the stable dynamic response of the vehicle suspension system during continuous vibrations. Figures 14 and 15 present the vertical acceleration signal in the front and rear seats in the original and modified configurations

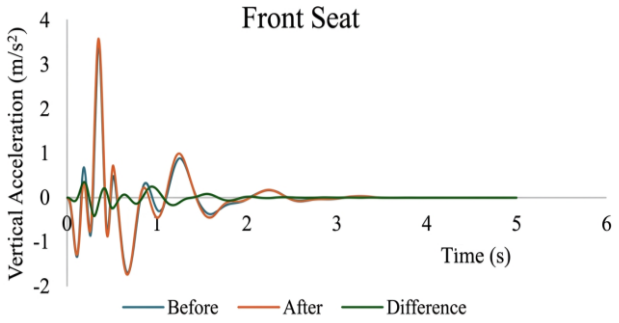


**Fig. 14 Vertical acceleration response at the front seating area due to a sinusoidal road profile (before, after, and difference)**

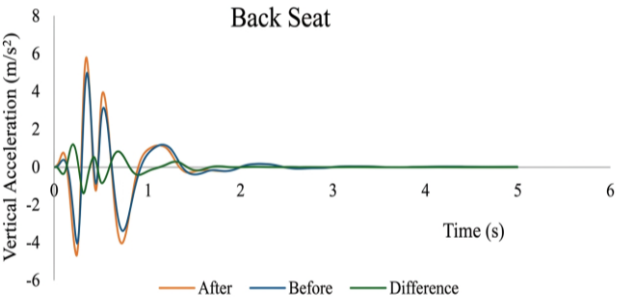


**Fig. 15 Vertical acceleration at the rear seat due to a sinusoidal road profile (before, after, and difference)**

The fourth evaluation considered a speed reducer profile developed from the geometric specifications established by the MTC guideline corresponding to a real driving excitation scenario.

This case produces the nature of transient excitation occurring in common driving situations. Figures 16 and 17 show the front and rear seat acceleration signals in the original and converted configurations.

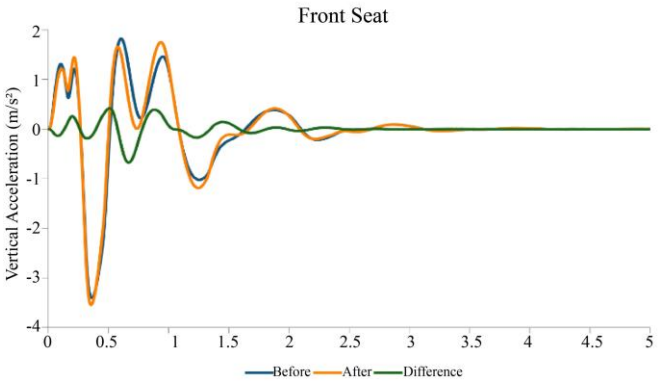


**Fig. 16 Vertical acceleration response at the front seating area due to a speed reducer profile (before, after, and difference)**

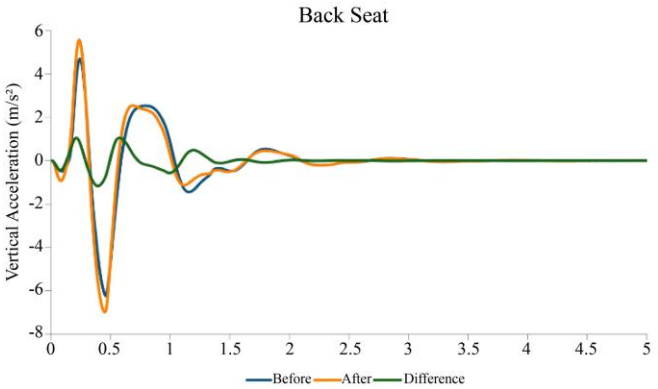


**Fig. 17 Vertical acceleration response at the rear seating area due to a speed reducer profile (before, after, and difference)**

### *4.1. Application of the Wk Weighting Filter (ISO 2631-1) in Simulink*

In order to comply with the evaluation requirements specified by ISO 2631-1 [37], the acceleration signals in the vertical direction obtained from the seating positions were analyzed with the Wk frequency weighting function, which corresponds to the human response sensitivity to vibrations in the vertical direction.

#### *4.1.1. Applying the Wk Filter in Simulink*

In the present study, the ISO Wk weighting was incorporated directly in the MATLAB/Simulink environment with a transfer function module. A rational approximation of the transfer function broadly adopted in previous studies was considered, allowing a precise reproduction of the frequency characteristics according to ISO 2631-1. The coefficients applied in the numerator are given as :

*[87.73, 1139, 11336, 5453, 5509]*

While at the same time, the coefficients of the denominator were established as:

*[1, 92.82, 2557, 25900, 81210, 79830],*

This implementation generates the weighted acceleration signal. $a_w(t)$, which accurately reflects passenger perception

of vibrations in the vertical direction. The resulting weighted acceleration signals for the two vehicle configurations (before and after modification) were later used to determine the Root Mean Square (RMS) acceleration and the VDV parameter, ensuring adherence to international comfort assessment regulations [11, 26]. The application of the Wk weighting function in the Simulink environment is shown in Figure 18.

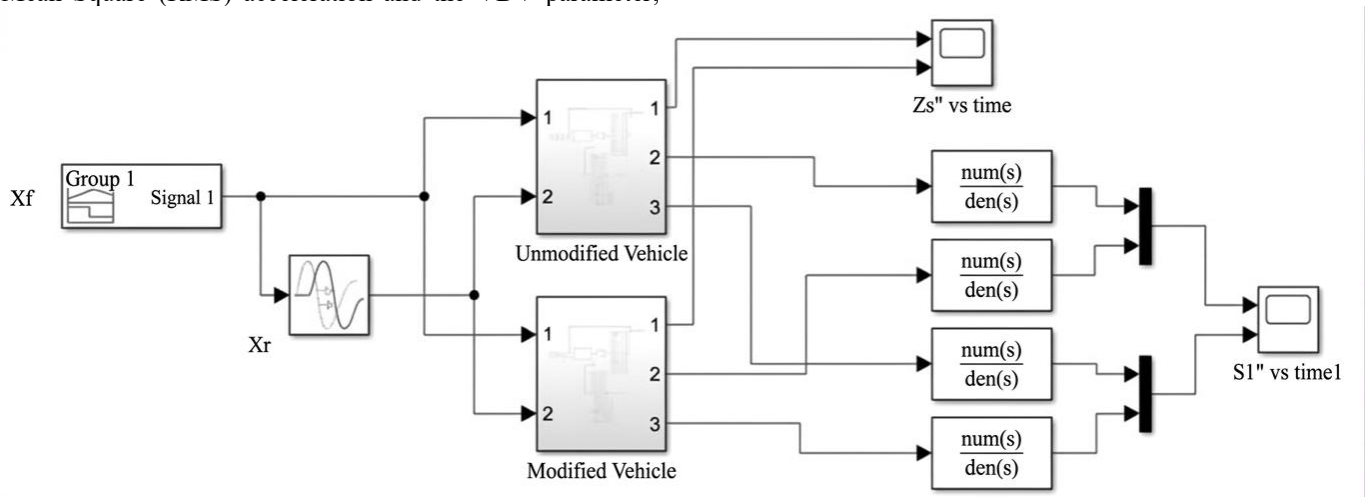


**Fig. 18 Transfer Fcn Block for Wk Filter**

*4.1.2. RMS*

To evaluate the amount of vibration transferred to the vehicle occupant, the root mean square metric of the weighted acceleration response was determined following the recommendations of ISO 2631-1. This metric reflects the effective vibration intensity during the evaluation period and is considered the principal metric for evaluating passenger comfort. When the filtered acceleration response is calculated by means of the Wk weighting filter, the Root Mean Square (RMS) value is determined as:

$$a_{RMS} = \sqrt{\frac{1}{T}\int_0^T (a_w(t))^2 dt} \tag{16}$$

In which $a_w(t)$ is the Wk-weighted vertical acceleration, and T is the total measurement duration.

In the case of discrete signals exported from MATLAB/Simulink for later processing, the RMS metric is determined as:

$$a_{RMS} = \sqrt{\frac{1}{T}\sum_{i=1}^{N} a_{w,i}^2 \Delta t_i} \tag{17}$$

Where $a_{w,i}$ is the weighted acceleration at the i-th sample, $\Delta t_i = t_i - t_{i-1}$ represents the actual sampling interval, and **N** is the total number of samples. This formulation enables uniform processing of irregularly sampled data.

This methodology was applied to the vehicle before and after modification, in addition to the seat positions at the front and rear. The resulting RMS metrics give a quantitative basis for evaluating vibration levels and analyzing the effect of the structural modification on vehicle ride comfort.

The time domain analysis results were combined through two additional indicators established in ISO 2631-1, the weighted acceleration RMS corresponding to continuous vibration conditions and the VDV parameter [11].

The combined application of both parameters is required because, while the RMS metric represents continuous vibration conditions, recent advanced studies report that RMS metrics can underestimate short-duration road disturbances because they average the responses over time.

As a result, the use of the VDV metric together with RMS is necessary in the present study because it offers a more representative assessment of passenger perception in non-stationary vibration scenarios characteristic of discrete road disturbances [23].

For the assessment of impact-dominated vibration inputs, the Vibration Dose Value (VDV) gives a more detailed assessment of the degradation in passenger comfort.

Table 6 shows a comparative overview of the calculated VDV metrics before (ICE) and after (EV) the structural conversion, taking into account the six analyzed cases and the front and rear seating locations. The percentage difference between configurations is included as well, making it possible to perform a numerical assessment of the effect caused by mass redistribution on the severity of vibrations.

Generally, the assessment based on VDV demonstrates that even though the retrofit enables EV operation, the changes in mass distribution and inertia negatively influence the vehicle's capacity to attenuate vibration energy, mainly during repeated or impact-type excitations

**Table 6. Vibration Dose Value (VDV) comparison by excitation profile**

| Excitation Profile | Position | VDV Before (ICE) | VDV After (EV) | Increase in Severity | Comfort Observation |
|---|---|---|---|---|---|
| Positive Bump | Front Seat | 2.6322 | 2.721 | 3.37% | Moderate increase in peaks. |
| | Rear Seat | 4.7191 | 5.4561 | 15.62% | Significant Deterioration. |
| Negative Bump | Front Seat | 1.4245 | 1.4553 | 2.16% | Minimal increase. |
| | Rear Seat | 2.3738 | 2.574 | 8.44% | Notorious deterioration in impacts. |
| Sinusoidal | Front Seat | 1.6766 | 1.7257 | 2.93% | Slight increase in cumulative dose. |
| | Rear Seat | 2.7992 | 3.29 | 17.53% | Most critical case. |
| Speed Reducer | Front Seat | 1.98 | 2.01 | 1.86% | Slight increase in cumulative dose. |
| | Rear Seat | 3.56 | 4.05 | 13.68% | Significant Deterioration. |

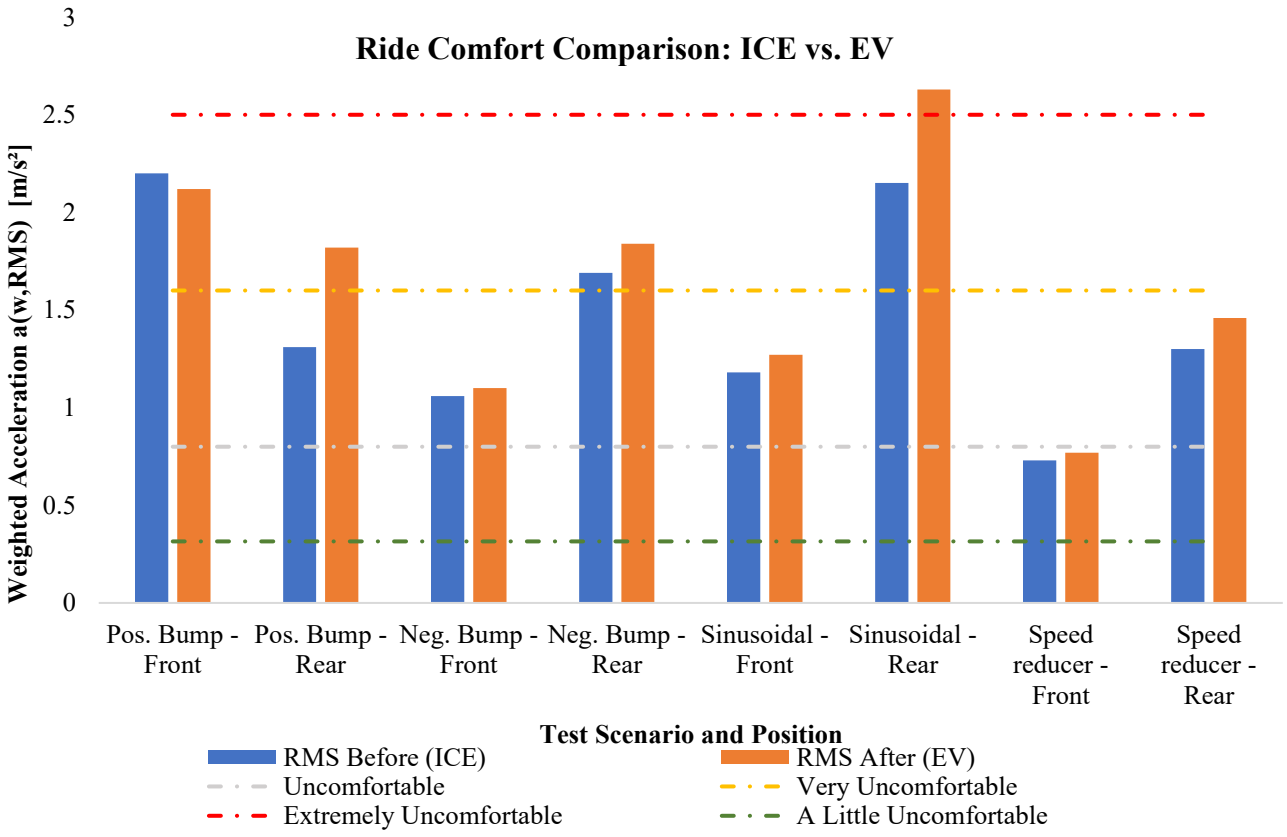


**Fig. 19 Comparative $a_{w,RMS}$ -Results Against ISO 2631-1 Comfort Thresholds**

*4.1.3. Weighted RMS Results (Wk)*

The Root Mean Square (RMS) weighted values of the vertical acceleration signal at both seating locations were assessed for both the original ICE vehicle and the converted Electric Vehicle (EV). Four disturbance cases were considered: upward bump excitation, downward road disturbance, sinusoidal disturbance profile, and the speed reducer excitation. The RMS value of the weighted acceleration corresponds to the effective vibration magnitude experienced by the occupant and is considered the principal comfort metric under continuous vibration exposure following ISO 2631-1 [11].

In the present study, the comfort evaluation ranges specified by the standard are employed as qualitative comparison zones to facilitate result interpretation instead of acting as rigid acceptability criteria [11, 27]. RMS acceleration values ranging approximately from 0.35 to 0.6 m/s² correspond to a slightly uncomfortable state, and RMS values ranging from 2.5 m/s² are related to high discomfort levels. [26, 28]

Under the positive road bump excitation from the seating position presents a small reduction in vibration intensity following the electric retrofit, from where the RMS decreases from 2.221 m/s² to 2.114 m/s². Even with this reduction, both RMS values stay in the very uncomfortable range, suggesting that the disturbance produces poor comfort conditions for both configurations. On the other hand, the rear siting position presents a notable rise in RMS values from 1.306 m/s² before modification to 1.814 m/s² after modification. This rise changes the comfort evaluation into the very uncomfortable category, indicating a reduction in ride comfort in the rear seating area in this excitation scenario.

For the negative bump case, the RMS at the front seat increases slightly from 1.061 m/s² to 1.097 m/s² after the conversion. The two values stay within the uncomfortable zone, showing that the conversion has only a small influence on the vibration response at the front seat during negative road excitations. In the rear seat area, the vibration level rises from 1.690 m/s² to 1.833 m/s², and both values stay in the very uncomfortable zone. This result confirms a repeated trend of higher vibration transmission toward the read seating position due to the redistributed mass caused by the conversion.

Under the sinusoidal road disturbance, the front seat shows an RMS increase from 1.177 m/s² in the original configuration to 1.270 m/s² after modification. While both results are inside the uncomfortable comfort zone, the variation shows a diminished capacity of the converted configuration to reduce periodic road disturbances. The rear seating position shows the most severe response of all analyzed scenarios, where the RMS rises from 2.146 m/s² to 2.631 m/s² after conversion. Even though the original setup already exhibits severe discomfort conditions, the covered vehicle approaches the extreme discomfort range (> 2.5 m/s²), demonstrating a major degradation in passenger comfort. This behavior shows that the retrofit negatively influences the dynamic of the real axle during repetitive excitations, possibly because of redistributed vehicle mass combined with limited suspension damping or stiffness to manage low-frequency dynamic motions.

In the speed humps scenario, the RMS value at the front seat increases from 0.73 m/s² to 0.76 m/s² after its conversion. The two results fall inside the slightly uncomfortable category, while the rear seating position shows an RMS increase from 1.3 m/s² to 1.46 m/s². Both RMS values correspond to uncomfortable conditions in the front and rear seats alike the obtained values demonstrate degradation in passenger comfort after electrification. The analysis demonstrates that in practical driving scenarios, like road speed bumps, passenger comfort becomes worse after electrification.

*4.1.4. Vibration Dose Value (VDV)*

The vibration dose value parameter, according to ISO 2631-1 [22, 38], is a parameter specifically designed to analyze the magnitude of impulsive vibration disturbances, including those caused by speed bumps, surface potholes, irregular surface transitions, or abrupt excitation conditions. In contrast to the Root Mean Square (RMS) value, which corresponds to the mean energy content of the filtered acceleration signal, the VDV is sensitive to peak accelerations by calculating the acceleration raised to the fourth power of the weighted vertical acceleration across the time interval.

Because of this mathematical formulation, the VDV is specially responsive to transient high-intensity vibration events, making it well-suited for studying vehicle dynamics to transient road inputs, including upward and downward bumps and discontinuous road surface inputs [39].
Based on ISO 2631-1, the vibration dose value is expressed as:

$$VDV = \left( \int_0^T |a_w(t)|^4 dt \right)^{1/4} \tag{18}$$

In which: $a_w(t)$ represents the vertical acceleration weighted with the Wk filter, while T represents the total exposure duration. The fourth-order formulation considerably amplifies the effect of peak accelerations, causing the VDV to respond strongly to transient vibration components.

From a practical perspective, larger VDV values represent stronger exposure to impulsive vibration disturbances, potentially causing reduced comfort, degraded ride quality, or increased physical stress on passengers based on the amplitude, exposure time, and frequency of occurrence of such vibrations. The VDV evaluation was conducted based on the weighted acceleration signals acquired from the front and rear seating locations in accordance with ISO 2631-1

standards. The obtained values are present in Table 7 for the unmodified and electric converted configurations, considering the four excitation scenarios analyzed in this work.

The findings show a continuous increase in Vibration Dose Values (VDV) levels in every profile after electrification, demonstrating a diminished ability of the converted vehicle suspension to damp high amplitude transient response.

The rear seating position presents considerably higher VDV values relative to the front seating position, showing reduced dynamic attenuation caused by changes in mass distribution and inertia impacting the rear suspension dynamics. Even though the positive bump causes the strongest transient loading, the most critical condition occurs for the rear seat under periodic excitation, where VDV reaches 3.29, confirming a substantial deterioration in comfort during repetitive disturbances.

**Table 7. Vibration Dose Value (VDV) results summary**

| Profile | Position | VDV Before | VDV After |
|---|---|---|---|
| Positive Bump | Front Seat | 2.6322 | 2.7210 |
| | Rear Seat | 4.7191 | 5.4561 |
| Negative Bump (Dip/Pothole) | Front Seat | 1.4245 | 1.4553 |
| | Rear Seat | 2.3738 | 2.5740 |
| Sinusoidal Profile | Front Seat | 1.6766 | 1.7257 |
| | Rear Seat | 2.7992 | 3.2900 |
| Speed Reducer Profile | Front Seat | 1.98 | 2.01 |
| | Rear Seat | 3.56 | 4.05 |

### *4.2. Qualitative Assessment of Model Parameters*

The transition from internal combustion propulsion to electric propulsion includes the extraction of the ICE powertrain and the incorporation of an electric drivetrain with battery modules. As noted by Arshad et al. and Yang et al. [19, 24], these changes strongly affect the weight distribution of the vehicle, potentially degrading passenger comfort if these effects are not carefully assessed.

Although a full optimization study is not included in the present work, a qualitative parametric analysis derived from the half-car dynamic equations between Equations (7) and (12) demonstrates how these changes impact the vibration response.

As presented in the results section, any variation in the Center of Gravity (CG) position directly modifies the distances $a$ and $b$. According to Equation (8), the overall pitching moment depends directly on the combined suspension and damping forces, considering their respective moment arms relative to the CG. While the gravitational force is applied at the center of gravity and consequently produces no rotational effect, any temporary imbalance between the front and rear suspension moments generates vehicle pitching.

In the modified configuration, while the pitch moment of inertia is reduced, the front and rear seats are located farther from the updated CG position. This positional shift intensifies the vertical dynamic accelerations at the passengers' locations during pitch motions.

As kinetic energy is proportional to velocity squared since velocity corresponds to the time integral of acceleration, any rise in these acceleration peaks results in a nonlinear increase in the dissipated energy, which the damping system is required to dissipate.

Additionally, with the CG displaced rearward, greater tire loading is required at the rear wheel contact points to balance the overall pitch moment defined in Equation (8). This greater load transfer, in combination with the inability of the stock dampers to dissipate the quadratic growth in vibration energy, causes the substantially higher RMS and VDV values obtained, especially at the rear seat.

### *4.3. Comparative Benchmarking with Factory EVs*

In the present section, the RMS results are evaluated in comparison with against previous research involving ride comfort studies of factory-built EVs. As presented in Table 8, the comparative analysis confirms a recurring global tendency associated with vehicle electrification, EV platforms naturally present increased RMS vibration values relative to conventional combustion vehicles.

This trend is validated according to the work of Yang et al. [40], demonstrating that electric propulsion modifies vibration behavior as a consequence of altered weight distribution and unsprung loads. In this present investigation, this tendency is validated in the context of vehicle electrification retrofits using the same chasses configuration (Ford Ka).

Despite differences in absolute vibration levels across studies because the present work focuses on discrete high impact disturbances including speed bumps relative to ISO Class B Road conditions the relative comfort deterioration follows the same tendency.

The analysis demonstrates that the retrofit process reflects the challenges associated with production EV's confirming the reliability of the proposed 6 DOF model demonstrating the essential requirement for suspension parameter recalibration to minimize the unfavorable impacts of the update mass inertia properties.

**Table 8. Comparative benchmarking of ride comfort (RMS Acceleration)**

| Vehicle Type | Power Source | Road Profile | RMS Acc. (m/s2) | Comfort Level (ISO 2631-1) |
|---|---|---|---|---|
| Traditional ICE [40] | Combustion | ISO Class B at 80 km/h | 0.658 | Fairly uncomfortable |
| Factory EV [40] | Electric (In-wheel) | ISO Class B at 80 km/h | 0.736 | Fairly uncomfortable |
| This Study (Baseline ICE) | Combustion | Speed reducer (60km/) | 0.73-1.3 | Uncomfortable |
| This Study (Retrofitted EV) | Electric | Speed reducer (60km/) | 0.77-1.46 | Uncomfortable |

### *4.4. Discussion of Results*

The joint evaluation of the RMS and vibration dose value metrics demonstrates that the EV retrofit changes not just the intensity but also the behavior of the vibrations perceived by occupants. While the RMS results demonstrate limited differences in mean vibration levels under specific disturbance profiles, the VDV metrics systematically reveal higher vibration severity after conversion, especially under transient and repetitive excitations.

The consistent increase in VDV, mainly in the rear seating position, shows a diminished ability of the converted vehicle to reduce high-intensity transient acceleration peaks. This trend is attributed to the changes in mass and inertia distribution caused by the electric powertrain integration, which modifies the interaction dynamics between the sprung mass, suspension components, and road inputs. For the sinusoidal road input case, the higher VDV further shows a greater accumulation of vibration energy during sustained periodic excitations, indicating an enhanced sensitivity of the modified vehicle to low-frequency dynamic excitations. In general the findings show that transient sensitive indicators metrics sensitive to transient vibrations, such as VDV, are essential for accurately capturing ride comfort degradation following electric conversion, as average-based metrics alone may not fully reflect the observed comfort deterioration.

## 5. Scope, Model Assumptions, and Future Research Directions

The dynamic assessment presented here was specifically designed to analyze ride comfort under representative high-severity conditions with the purpose of determining the influence of changes in mass distribution resulting from EV conversion on the transmission of vertical vibrations [24]. The modeling assumptions and excitation conditions used were established to provide a reliable and safety-oriented analysis instead of attempting to reduce the estimated response.

A half-car model with six degrees of freedom was adopted as it adequately captures the main vertical dynamic behavior controlling ride comfort and permits direct comparison between the original and converted configurations. This model explicitly incorporates vertical translational motion and longitudinal pitch motion (front real rotational dynamics), which represent the dominant vibration modes governing human vibration exposure under longitudinal driving scenarios [17]. Side-to-side dynamics and roll motion related to left-right load transfer and uneven wheel excitations were excluded [28]. The omission of roll does not affect the reliability of the conclusions for ride comfort analysis in the vertical direction under balanced road disturbances, which are the dominant contributors to passenger discomfort based on ISO 2631-1 guidelines [15, 26]. The suspension and tire systems were represented with linear, stiffened, and damped assumptions. This assumption was purposefully used to ensure model interpretability and to avoid accounting for nonlinear effects that could distort the direct effects of mass and inertia variations resulting from EV conversion [14, 22]. Under this simplified formulation, any variation in RMS and VDV values can be directly linked to the impact of EV conversion, making it possible to have a transparent and physically interpretable analysis.

In addition, the analyzed excitation inputs, positive and negative step disturbances, sinusoidal inputs, and speed bump excitations were selected as key loading conditions able to produce significant transient and cyclic responses [28]. These excitation profiles are widely applied to simulate severe road disturbances, including bumps, potholes, and uneven road patterns, making sure that the studied cases correspond to high-demand operating conditions rather than representing ideal comfort scenarios [13, 15].

This analysis follows a deterministic approach. The dynamic response of the converted vehicle is evaluated for four distinct road excitations, under the assumption that the dominant influence on riding comfort in retrofitted electric vehicles is the redistribution of the sprung mass and the resulting shift in the center of gravity. The methodology was organized to capture these coupled phenomena, pitch and heave motions, through a 6-degree-of-freedom mathematical model and well-established ISO 2631-1 standards.

Future work should be viewed as optimization and improvement efforts instead of additional studies to find harsher conditions. As described in the previous section, the battery layout and DC motor must be designed to minimize the moment of inertia, which contributes to lower vibrations. For this reason, future studies may focus on studying the influence of battery system layout, including module count, weight, and spatial arrangement, on the dynamic behavior of the suspension system. In addition, this study highlights that

while traditional active suspension systems constitute a highly efficient approach for improving ride comfort, their performance and tuning methods critically depend on a precise characterization of the vehicle's physical properties [19, 20, 24]. As a result, future studies should prioritize the recalculation of key parameters such as the shifted center of gravity and the higher pitch inertia in order to ensure that control strategies are properly calibrated to the dynamics of the electrified chassis. In addition, the use of three-dimensional full vehicle models, nonlinear suspension dynamics, and physical validation can increase prediction precision. Suspension optimization and recalibration strategies, specifically stiffness and damping parameter adjustments using Particle Swarm Optimization (PSO) or Genetic Algorithms (GA) [17, 20], may be implemented to reduce the deterioration of comfort reported in this study. Additionally, modern active suspension systems based on Neural Networks and Reinforcement Learning for real-time adaptive control represent a promising approach to adaptively compensate for the specific inertial changes of converted electric vehicles [13, 20].

While this work uses objective ISO 2631-1 vibration metrics (such as RMS and VDV), a key limitation is the lack of direct assessments of perceived comfort, such as user questionnaires. As reported in recent advanced literature, defining direct quantitative relationships between mechanical vibration parameters and perceived comfort continues to be difficult [11]. In addition, although classical ISO standards provide a basic classification of discomfort, studies emphasize that human perception involves intrinsic variability and ambiguity [10]. The comfort perception is strongly subjective, differing substantially between people [27]. As a result, an essential next step will involve validation through human participant experiments to overcome the lack of comparison between measured vibration responses and perceived comfort data. Upcoming experiments will employ human-in-the-loop driving simulators or on-road testing with the EV converted vehicle. In such studies, measured multi-directional acceleration signals will be recorded concurrently and correlated with perceived discomfort scores obtained using standardized surveys including 7-point Likert rating scales [11, 27]. This combined objective- subjective approach will make possible a more refined calibration of the 6 DOF vehicle model and robust validation of the ride quality of the vehicle [11].

## 6. Conclusion

This work presents a numerical evaluation of the effect of electric conversion on vertical vibration behavior and comfort of a Ford Ka vehicle. The retrofit process, the integration of a battery system and electric motor, substantially changed the mass and inertia properties of the vehicle, directly impacting the propagation of road-generated vibrations via the suspension system.

To evaluate this effect, a half-car model with six degrees of freedom was developed and numerically simulated in MATLAB/Simulink. The system response was analyzed under four different excitation profiles: a positive step, a negative step, a sinusoidal input, and a speed reducer input (speed bump excitation). Following ISO 2631-1, the calculated vertical accelerations at the occupant position in the front and rear seats were processed using the Wk. weighting filter with the RMS value of weighted acceleration ($a_{w,RMS}$) and the VDV metric acting as a key ride comfort metric.

The analysis indicates a systematic deterioration in ride comfort after the electric conversion. Both RMS and VDV values rose in most excitation cases, with the greatest reduction in comfort observed in the rear seat, where VDV rose by as much as 17.5% during sinusoidal loading. This result demonstrates that the mass redistribution caused by the retrofit reduces the suspension's capacity to attenuate vibrations, especially short-duration and impact-type events, which are strongly represented by the VDV indicator. Although the conversion achieves its main goal of electrification, the results highlight that it does not retain the initial vehicle's dynamic comfort. The factory suspension system was tuned for a different mass and inertia distribution; as a result, the changed dynamics led to increased vibration exposure for occupants. This result highlights an important design trade-off and makes necessary the implementation of suspension recalibration or optimization, particularly targeting stiffness and damping properties as a necessary step in the electrification process to recover acceptable ride quality.

The approach used in this work, combining a Six Degree of Freedom model, time domain simulations, and ISO 2632-1, was effective in describing the vertical dynamic effects of changes in mass distribution in EV converted vehicles. As a result, this study demonstrates that complete ride comfort assessment must be an essential component of the design and verification phases in vehicle electrification projects so that the shift to electric mobility does not negatively affect occupant comfort and perceived quality.

## Conflicts of Interest

The authors confirm that there are no conflicts of interest concerning the publication of this article.

## Funding Statement

The authors did not receive external financial support for the research, authorship, or publication of this article.

## Acknowledgements

Sincere gratitude is extended to the Universidad Nacional de San Agustín de Arequipa for its support and the knowledge provided. Special thanks are also extended to Claudia Ponce and Andre Tavares (Electrical Engineering – Centro Universitário – UNISATC, Brazil) for their valuable contributions.

## References


[1] Hao Mu, and Rui Xiong, "Modeling, Evaluation, and State Estimation for Batteries," *Modeling, Dynamics, and Control of Electrified Vehicles*, pp. 1-38, 2018. [CrossRef] [Google Scholar] [Publisher Link]

[2] Gabriel Domingues, Avo Reinap, and Mats Alaküla, "Design and Cost Optimization of Electrified Automotive Powertrain," *2016 International Conference on Electrical Systems for Aircraft, Railway, Ship Propulsion and Road Vehicles & International Transportation Electrification Conference (ESARS-ITEC)*, Toulouse, France, pp. 1-6, 2016. [CrossRef] [Google Scholar] [Publisher Link]

[3] André Abelardo Tavares et al., "Power Losses Analysis and Efficiency Evaluation of an Electric Vehicle Conversion," Power Losses Analysis and Efficiency Evaluation of an Electric Vehicle Conversion," *2018 IEEE International Conference on Electrical Systems for Aircraft, Railway, Ship Propulsion and Road Vehicles & International Transportation Electrification Conference (ESARS-ITEC)*, Nottingham, UK, pp. 1-6, 2018. [CrossRef] [Google Scholar] [Publisher Link]

[4] 2017 Brazilian Automotive Industry Yearbook, Anfavea, National Association of Motor Vehicle Manufacturers, 2017. [Online]. Available: https://anfavea.com.br/anuario2017/Anfavea_2017.pdf

[5] 2018 Brazilian Automotive Industry Yearbook, Anfavea, National Association of Motor Vehicle Manufacturers, 2018. [Online]. Available: https://anfavea.com.br/anuario2018/Anfavea_18.pdf

[6] 2019 Brazilian Automotive Industry Yearbook, Anfavea, National Association of Motor Vehicle Manufacturers, 2019. [Online]. Available: https://www.anfavea.com.br/anuario2019/anuario.pdf

[7] 2020 Brazilian Automotive Industry Yearbook, Anfavea, National Association of Motor Vehicle Manufacturers, 2020. [Online]. Available: https://www.anfavea.com.br/anuario2020/site/anuario_2020.pdf

[8] Pang Hui, Liu Fan, and Xu Zeren, "Variable Universe Fuzzy Control for Vehicle Semi-Active Suspension System with MR Damper Combining Fuzzy Neural Network and Particle Swarm Optimization," *Neurocomputing*, vol. 306, pp. 130-140, 2018. [CrossRef] [Google Scholar] [Publisher Link]

[9] Mirko Gordić et al., "Electric Vehicle Conversion: Optimisation of Parameters in the Design Process," *Technical Journal*, vol. 24, no. 4, pp. 1213-1219, 2017. [CrossRef] [Google Scholar] [Publisher Link]

[10] Xiaojuan Wang et al., "Human Response to Vibrations and Its Contribution to the Overall Ride Comfort in Automotive Vehicles - A Literature Review," *WCX SAE World Congress Experience, Detroit*, Michigan, United States, 2020. [CrossRef] [Google Scholar] [Publisher Link]

[11] Cornelia Stan, and Razvan Andrei Oprea, "Vibration Comfort Assessment Methods in Heavy Vehicles: Models, Standards and Numerical Approaches—A State-of-the-Art Review," *Technologies*, vol. 14, no. 2, pp. 1-28, 2026. [CrossRef] [Google Scholar] [Publisher Link]

[12] Jing Na et al., "Active Suspension Control of Quarter-Car System with Experimental Validation," *IEEE Transactions on Systems, Man, and Cybernetics: Systems*, vol. 52, no. 8, pp. 4714-4726, 2022. [CrossRef] [Google Scholar] [Publisher Link]

[13] Kyle Samaroo et al., "Performance Investigation of Active, Semi-Active and Passive Suspension Using Quarter Car Model," *Algorithms*, vol. 18, no. 2, pp. 1-19, 2025. [CrossRef] [Google Scholar] [Publisher Link]

[14] Ganesh D. Shelke, Anirban C. Mitra, and Vinay R. Varude, "Validation of Simulation and Analytical Model of Nonlinear Passive Vehicle Suspension System for Quarter Car," *Materials Today: Proceedings*, vol. 5, no. 9, pp. 19294-19302, 2018. [CrossRef] [Google Scholar] [Publisher Link]

[15] Raj Desai, Anirban Guha, and P. Seshu, "A Comparison of Quarter, Half and Full Car Models for Predicting Vibration Attenuation of an Occupant in a Vehicle," *Journal of Vibration Engineering & Technologies*, vol. 9, pp. 983-1001, 2021. [CrossRef] [Google Scholar] [Publisher Link]

[16] Mehrullah Soomro, Mohd Khair Hassan, and Fauzi Ahmad, "Modelling and Validation of An Electronic Wedge Brake System with Realistic Quarter Car Model for Anti-Lock Braking System Design," *International Journal of Integrated Engineering*, vol. 11, no. 4, pp. 70-80, 2019. [CrossRef] [Google Scholar] [Publisher Link]

[17] Maria-Geanina Unguritu, Teodor-Constantin Nichit¸elea, and Dan Selis¸teanu, "Design and Performance Assessment of Adaptive Harmonic Control for a Half-Car Active Suspension System," *Complexity*, vol. 2022, no. 1, pp. 1-14, 2022. [CrossRef] [Google Scholar] [Publisher Link]

[18] Herman A. Hamersma, and Schalk Els, "A Comparison of Quarter, Half and Full Vehicle Models With Experimental Ride Comfort Data," *Proceedings of the ASME 2015 International Design Engineering Technical Conferences and Computers and Information in Engineering Conference*, vol. 3, pp. 1-7, 2015. [CrossRef] [Google Scholar] [Publisher Link]

[19] Muhammad Waqas Arshad, Stefano Lodi, and David Q. Liu, "Multi-Objective Optimization of Independent Automotive Suspension by AI and Quantum Approaches: A Systematic Review," *Machines*, vol. 13, no. 3, pp. 1-31, 2025. [CrossRef] [Google Scholar] [Publisher Link]

[20] Yixin Mei et al., "Classification Evolution, Control Strategy Innovation, and Future Challenges of Vehicle Suspension Systems: A Review," *Actuators*, vol. 14, no. 10, pp. 1-33, 2025. [CrossRef] [Google Scholar] [Publisher Link]

[21] Mohamed Issa, and Anas Samn, "Passive Vehicle Suspension System Optimization using Harris Hawk Optimization Algorithm," *Mathematics and Computers in Simulation*, vol. 191, pp. 328-345, 2022. [CrossRef] [Google Scholar] [Publisher Link]

[22] Anirban. C. Mitra et al., "Optimization of Passive Vehicle Suspension System by Genetic Algorithm," *Procedia Engineering*, vol. 144, pp. 1158-1166, 2016. [CrossRef] [Google Scholar] [Publisher Link]

[23] Alicja Kowalska-Koczwara et al., "Assessing the Influence of RMS and VDV on Analysis of Human Perception of Vibrations in Buildings Caused by Selected Sources of Traffic," *Applied Sciences*, vol. 14, no. 9, pp. 1-17, 2024. [CrossRef] [Google Scholar] [Publisher Link]

[24] Zheng Yang et al., "Simulation Analysis and Optimization of Ride Quality of In-Wheel Motor Electric Vehicle," *Advances in Mechanical Engineering*, vol. 10, no. 5, pp. 1-10, 2018. [CrossRef] [Google Scholar] [Publisher Link]

[25] H. Mazumder, M. Ektesabi, and A. Kapoor, "Effect of Mass Distribution on Cornering Dynamics of Retrofitted EV," *2012 IEEE International Electric Vehicle Conference*, Greenville, SC, USA, pp. 1-6, 2012. [CrossRef] [Google Scholar] [Publisher Link]

[26] Guichun Wang, Jie Zhang, and Xuan Kong, "Study on Passenger Comfort Based on Human–Bus–Road Coupled Vibration," *Applied Sciences*, vol. 10, no. 9, pp. 1-22, 2020. [CrossRef] [Google Scholar] [Publisher Link]

[27] Georg Burkhard et al., "An Extended Model of the ISO-2631 Standard to Objectify the Ride Comfort in Autonomous Driving," *Work: A Journal of Prevention, Assessment & Rehabilitation*, vol. 68, no. s1, pp. S37-S45, 2021. [CrossRef] [Google Scholar] [Publisher Link]

[28] Y. Susatio et al., "Design of Half-Car Active Suspension System for Passenger Riding Comfort," *Journal of Physics: Conference Series*, vol. 1075, 2018. [CrossRef] [Google Scholar] [Publisher Link]

[29] Omar Zamzam et al., "Structural Performance Evaluation of Electric Vehicle Chassis under Static and Dynamic Loads," *Scientific Reports*, vol. 15, pp. 1-20, 2025. [CrossRef] [Google Scholar] [Publisher Link]

[30] Bing Liu, Mehrdad Saif, and Huijin Fan, "Adaptive Fault Tolerant Control of a Half-Car Active Suspension Systems Subject to Random Actuator Failures," *IEEE/ASME Transactions on Mechatronics*, vol. 21, no. 6, pp. 2847-2857, 2016. [CrossRef] [Google Scholar] [Publisher Link]

[31] A.E. Geweda et al., "Improvement of Vehicle Ride Comfort Using Genetic Algorithm Optimization and PI Controller," *Alexandria Engineering Journal*, vol. 56, no. 4, pp. 405-414, 2017. [CrossRef] [Google Scholar] [Publisher Link]

[32] Syed M. Hur Rizvi et al., "H∞ Control of 8 Degrees of Freedom Vehicle Active Suspension System," *Journal of King Saud University - Engineering Sciences*, vol. 30, no. 2, pp. 161-169, 2018. [CrossRef] [Google Scholar] [Publisher Link]

[33] Ministry of Transport and Communications, Directorial Resolution No. 023-2011-MTC/14, Bump Type Speed Reducers for the National Highway System (SINAC), gob.pe, 2011. [Online]. Available: https://www.gob.pe/institucion/mtc/normas-legales/282284-023-2011-mtc-14

[34] Muna Alqam, and Faical Mnif, "Simulation and Analysis using Matlab and Simulink® of a Car Suspension System Model Under Different Road Conditions: A Project-based Learning Approach," *2024 21st International Multi-Conference on Systems, Signals & Devices (SSD)*, Erbil, Iraq, pp. 798-804, 2024. [CrossRef] [Google Scholar] [Publisher Link]

[35] Khoi Nguyen Nguyen, and Ngoc Vy Duong, "Evaluation of Longitudinal Ride Comfort of an Electric Vehicle Using Matlab/Simulink," *European Journal of Automated Systems*, vol. 58, no. 7, pp. 1327-1333, 2025. [CrossRef] [Google Scholar] [Publisher Link]

[36] Srivatsan Srinivasan, 6 DoF Vehicle Model in Simulink, MATLAB Central File Exchange, 2021. [Online]. Available: https://www.mathworks.com/matlabcentral/fileexchange/70497-6-dof-vehicle-model-in-simulink

[37] Anandika Parwata, and Wiwiek Hendrowati, "Optimization of Dynamic Vibration Absorber on Ambulance Stretchers Using the Genetic Algorithm Method Based on ISO 2631 Standards," *Engineering Proceedings*, vol. 84, no. 1, pp. 1-18, 2025. [CrossRef] [Google Scholar] [Publisher Link]

[38] Damian Frej, "Analysis of Vibration Comfort and Vibration Energy Distribution in the Child Restraint System-Base Configuration," *Energies*, vol. 18, no. 19, pp. 1-38, 2025. [CrossRef] [Google Scholar] [Publisher Link]

[39] Peter Múčka, "Vibration Dose Value in Passenger Car and Road Roughness," *Journal of Transportation Engineering, Part B: Pavements*, vol. 146, no. 4, 2020. [CrossRef] [Google Scholar] [Publisher Link]

[40] Fuxing Yang et al., "Analytical Description of Ride Comfort and Optimal Damping of Cushion-Suspension for Wheel-Drive Electric Vehicles," *International Journal of Automotive Technology*, vol. 18, pp. 1121-1129, 2017. [CrossRef] [Google Scholar] [Publisher Link]